Supplementary Information
Endogenous environmental volatility creates multistability and oscillations in evolutionary games

Hao Yu and Junjie Fu

Abstract

This Supplementary Information derives the strategy–volatility model from an exact finite-population birth–death process, records all scaling assumptions, and supplies the algebra and numerical controls supporting the main text. We retain a general payoff-sensitivity matrix $B \neq A$, derive the quartic coexistence polynomial and its coefficients, give boundary and interior stability conditions, state the Hopf and first-Lyapunov-coefficient conventions, and document finite-population diffusion. Additional analyses establish robustness to non-proportional sensitivity, shock distribution, population size, weak selection and numerical tolerances. No displayed equation is framed or boxed; symbols are used consistently with the main manuscript.

Contents

1 Model hierarchy and notation

The construction separates three sources or time scales of variation. A fast random variable ξ_τ changes realized payoffs before every microscopic update. A slow non-negative state κ_τ controls the amplitude of those shocks and responds to population composition. Finite sampling of parents and replaced individuals generates demographic randomness. The first two mechanisms survive in the deterministic large-population drift, whereas the third appears as a finite-N diffusion.

The population contains $n \in \{0, \dots, N\}$ cooperators and $N - n$ defectors, with $x = n/N$. Rows of the mean payoff matrix A index the focal strategy and columns index the opponent,

$$A = \begin{pmatrix} a & b \\ c & d \end{pmatrix}, \qquad B = \begin{pmatrix} \alpha & \beta \\ \gamma & \delta \end{pmatrix}. \tag{S1.1}$$

The second matrix specifies sensitivity to a common environmental shock and need not be proportional to A. In the large-N limit, the cooperator–defector mean payoff difference and sensitivity difference are

$$\Delta(x) = (b - d) + (a - b - c + d)x = F + Gx, \tag{S1.2}$$

$$\Gamma(x) = (\beta - \delta) + (\alpha - \beta - \gamma + \delta)x = P + Qx. \tag{S1.3}$$

Thus $F = \Delta(0)$ and $F + G = \Delta(1)$ characterize mean invasion incentives, while $P = \Gamma(0)$ and $P + Q = \Gamma(1)$ characterize differential exposure to the fast environment. The target volatility is

$$\Psi(x) = (1 - x)\kappa_{\mathrm{D}} + x\kappa_{\mathrm{C}} = \kappa_{\mathrm{D}} + hx, \qquad h = \kappa_{\mathrm{C}} - \kappa_{\mathrm{D}}. \tag{S1.4}$$

Cooperation buffers variability when $h < 0$ and amplifies it when $h > 0$. Table S1 summarizes the principal quantities.

Supplementary Table S1: Principal notation.

Symbol	Meaning
N, n, x	population size, cooperator count and cooperator frequency n/N
A, B	mean payoff matrix and environmental sensitivity matrix
s	microscopic selection strength
ξ_τ	independent centered, unit-variance fast payoff shock
κ	scaled environmental volatility
F, G	intercept and slope of the mean payoff difference $\Delta(x)$
P, Q	intercept and slope of the sensitivity difference $\Gamma(x)$
$\kappa_{\mathrm{D}}, \kappa_{\mathrm{C}}$	target volatility at all defection and all cooperation
h	strategy feedback contrast $\kappa_{\mathrm{C}} - \kappa_{\mathrm{D}}$
ε	environmental relaxation rate in macroscopic event time
ω	response ratio ε/s in selection time
θ	selection time $s\tau/N$

2 Finite-population microscopic process

2.1 Realized payoffs

Before event τ, an independent shock is drawn with $\mathbb{E}\xi_\tau = 0$ and $\mathbb{E}\xi_\tau^2 = 1$. The realized game is

$$A_\tau = A + \xi_\tau \sqrt{\frac{\kappa_\tau}{s}} B. \tag{S2.1}$$

The $s^{-1/2}$ amplitude is a deliberate weak-selection scaling. It makes the deterministic payoff contrast $s\Delta$ and the variance contribution $s\kappa\Gamma^2$ enter the averaged drift at the same order. With no self-interaction, the realized payoffs are

$$\Pi_\mathrm{C} = \frac{(n-1)A_{\tau,CC} + (N-n)A_{\tau,CD}}{N-1}, \tag{S2.2}$$

$$\Pi_\mathrm{D} = \frac{nA_{\tau,DC} + (N-n-1)A_{\tau,DD}}{N-1}. \tag{S2.3}$$

Their difference can be written as a deterministic finite-N term plus a shock sensitivity term. Both converge to $\Delta(x)$ and $\Gamma(x)$ as $N \to \infty$; the exact finite-N expressions are used in all microscopic calculations.

2.2 Birth–death transition kernel

Fitness is exponential, $f_i = \exp(s\Pi_i)$, ensuring positivity. A parent is selected in proportion to fitness and replaces a uniformly selected different individual. Conditional on ξ_τ,

$$T^+(n, \kappa \mid \xi) = \frac{nf_\mathrm{C}}{nf_\mathrm{C} + (N-n)f_\mathrm{D}} \frac{N-n}{N-1}, \tag{S2.4}$$

$$T^-(n, \kappa \mid \xi) = \frac{(N-n)f_\mathrm{D}}{nf_\mathrm{C} + (N-n)f_\mathrm{D}} \frac{n}{N-1}. \tag{S2.5}$$

The remaining probability corresponds to no change in n. Define the log-fitness contrast $u = s(\Pi_\mathrm{C} - \Pi_\mathrm{D})$. Then

$$T^+ - T^- = \frac{Nx(1-x)}{N-1} \frac{e^u - 1}{xe^u + 1 - x}. \tag{S2.6}$$

This expression makes clear why averaging the payoff before applying selection is incorrect: the transition probability is nonlinear in u.

2.3 Environmental update

After the strategy event, the slow state follows

$$\kappa_{\tau+1} = \kappa_\tau + \frac{\varepsilon}{N} \left[\Psi(x_\tau) - \kappa_\tau\right]. \tag{S2.7}$$

When $0 < \varepsilon/N \leq 1$ and $\kappa_{\mathrm{D}}, \kappa_{\mathrm{C}} \geq 0$, Eq. (S2.7) is a convex combination of non-negative quantities. The microscopic process therefore preserves $\kappa \geq 0$.

3 Weak-selection reduction

3.1 Expansion of the exact drift

The nonlinear factor in Eq. (S2.6) has the Taylor series

$$\frac{e^u - 1}{xe^u + 1 - x} = u + \left(\frac{1}{2} - x\right) u^2 + \mathcal{O}(u^3). \tag{S3.1}$$

For the scaling in Eq. (S2.1), the large-N log-fitness contrast is

$$u = s\Delta(x) + \sqrt{s\kappa}\,\Gamma(x)\xi. \tag{S3.2}$$

Consequently, $\mathbb{E}u = s\Delta$ and $\mathbb{E}u^2 = s\kappa\Gamma^2 + s^2\Delta^2$. Substitution into Eq. (S3.1), multiplication by the event rate N, and retention of the leading order give

$$\frac{\mathrm{d}x}{\mathrm{d}t} = sx(1-x)\left[\Delta(x) + \left(\frac{1}{2} - x\right)\kappa\Gamma^2(x)\right] + \mathcal{O}(s^2) + \mathcal{O}(N^{-1}), \tag{S3.3}$$

where $t = \tau/N$. Thus a centered shock generates non-zero selection through its second moment. The sign change at $x = 1/2$ results from the asymmetry of competitive replacement, not from an asymmetric shock distribution.

3.2 Demographic diffusion

At neutrality, $T^+ + T^- = 2Nx(1-x)/(N-1)$. The one-event variance therefore satisfies

$$N^2\,\mathrm{Var}(\Delta x) = \frac{2N}{N-1}x(1-x) + \mathcal{O}(s), \tag{S3.4}$$

which approaches $2x(1-x)$. In event time, the variance rate is $2x(1-x)/(N-1)$ to leading order. Rescaling to selection time $\theta = st$ gives the Itô system

$$\mathrm{d}x = x(1-x)\left[\Delta(x) + \left(\tfrac{1}{2} - x\right)\kappa\Gamma^2(x)\right]\mathrm{d}\theta + \sqrt{\frac{2x(1-x)}{s(N-1)}}\,\mathrm{d}W_\theta, \tag{S3.5}$$

$$\mathrm{d}\kappa = \omega[\kappa_{\mathrm{D}} + hx - \kappa]\mathrm{d}\theta, \tag{S3.6}$$

with $\omega = \varepsilon/s$. Replacing $N-1$ by N gives the leading large-N expression used in the main text. The deterministic interior approximation requires weak selection and sufficiently large effective size, with demographic fluctuations small on the observation interval.

3.3 Distributional universality and its limits

At the retained order, the shock distribution enters only through $\mathbb{E}\xi = 0$ and $\mathbb{E}\xi^2 = 1$. Gaussian, Rademacher, uniform and Laplace shocks therefore share the same leading drift. Their different skewness and kurtosis affect terms beyond the order retained here. The numerical comparison in Supplementary Fig. S2 verifies that these differences shrink with s. The conclusion does not cover shocks with undefined variance or temporal correlations whose correlation time remains finite on the macroscopic scale.

4 General deterministic strategy–volatility system

Dropping the demographic term in Eq. (S3.6) gives

$$x' = X(x)S(x,\kappa), \qquad X(x) = x(1-x), \tag{S4.1}$$

$$S(x,\kappa) = F + Gx + \left(\tfrac{1}{2} - x\right)\kappa(P+Qx)^2, \tag{S4.2}$$

$$\kappa' = \omega(\kappa_{\mathrm{D}} + hx - \kappa). \tag{S4.3}$$

The state rectangle $0 \le x \le 1$, $\kappa \ge 0$ is positively invariant. At $x = 0$ or $x = 1$, $x' = 0$. At $\kappa = 0$, the environmental component is $\omega(\kappa_{\mathrm{D}} + hx) = \omega\Psi(x) \ge 0$ when the endpoint targets are non-negative.

4.1 Boundary equilibria and invasion conditions

The two boundary equilibria are $P_{\mathrm{D}} = (0, \kappa_{\mathrm{D}})$ and $P_{\mathrm{C}} = (1, \kappa_{\mathrm{C}})$. Their environmental eigenvalue is always $-\omega$. The strategy eigenvalues are

$$\lambda_{\mathrm{D}} = F + \frac{1}{2}\kappa_{\mathrm{D}}P^2, \tag{S4.4}$$

$$\lambda_{\mathrm{C}} = -\left[F + G - \frac{1}{2}\kappa_{\mathrm{C}}(P+Q)^2\right]. \tag{S4.5}$$

Thus all defection is locally stable when $F + \kappa_{\mathrm{D}}P^2/2 < 0$, while all cooperation is locally stable when $F + G - \kappa_{\mathrm{C}}(P+Q)^2/2 > 0$. Volatility changes invasion criteria even though the fast shock has zero mean.

4.2 Interior equilibrium polynomial

At an interior equilibrium, $\kappa = \kappa_{\mathrm{D}} + hx$ and $S = 0$. Defining

$$\mathcal{F}(x) = F + Gx + \left(\tfrac{1}{2} - x\right)(\kappa_{\mathrm{D}} + hx)(P+Qx)^2, \tag{S4.6}$$

the physical roots satisfy $0 < x < 1$ and $\kappa_{\mathrm{D}} + hx > 0$. Write $(\frac{1}{2} - x)(\kappa_{\mathrm{D}} + hx) = a_0 + a_1x + a_2x^2$, where $a_0 = \kappa_{\mathrm{D}}/2$, $a_1 = h/2 - \kappa_{\mathrm{D}}$ and $a_2 = -h$. Then

$$\mathcal{F}(x) = c_0 + c_1x + c_2x^2 + c_3x^3 + c_4x^4, \tag{S4.7}$$

with

$$c_0 = F + a_0P^2, \tag{S4.8}$$
$$c_1 = G + 2a_0PQ + a_1P^2, \tag{S4.9}$$
$$c_2 = a_0Q^2 + 2a_1PQ + a_2P^2, \tag{S4.10}$$
$$c_3 = a_1Q^2 + 2a_2PQ, \tag{S4.11}$$
$$c_4 = a_2Q^2 = -hQ^2. \tag{S4.12}$$

The general model can therefore have at most four isolated interior equilibria. Degeneracies reduce the degree: $h = 0$ or $Q = 0$ gives at most a cubic, and further parameter identities can reduce it again.

5 Proportional sensitivity as a factorized special case

If $B = A$, then $P = F$, $Q = G$ and $\Gamma = \Delta = D(x)$. Equation (S4.3) factorizes as

$$x' = x(1-x)D(x)\left[1 - \kappa\left(x - \tfrac{1}{2}\right)D(x)\right], \qquad \kappa' = \omega(\kappa_{\mathrm{D}} + hx - \kappa). \tag{S5.1}$$

Interior states consist of the classical mixed root $D(x) = 0$ and the variance-induced roots of

$$H(x) = (\kappa_{\mathrm{D}} + hx)\left(x - \tfrac{1}{2}\right)(F + Gx) - 1 = 0. \tag{S5.2}$$

The induced condition is cubic when $hG \neq 0$, so the proportional system can have the classical root plus three induced roots. Physical induced roots automatically have $\kappa = \kappa_{\mathrm{D}} + hx > 0$ and require $(x - 1/2)D(x) > 0$.

When $\kappa = 0$, Eq. (S5.1) reduces to the ordinary replicator equation. When $h = 0$, volatility relaxes to a constant and the system becomes triangular after the transient in κ. When $G = 0$, the proportional model lacks the frequency dependence required for the response-rate Hopf mechanism derived below.

6 Jacobian and local stability

For the general system, derivatives of the selection factor are

$$S_x = G + \kappa\left[-\Gamma^2 + 2\left(\tfrac{1}{2} - x\right)Q\Gamma\right], \tag{S6.1}$$
$$S_\kappa = \left(\tfrac{1}{2} - x\right)\Gamma^2. \tag{S6.2}$$

The Jacobian is

$$J = \begin{pmatrix} (1-2x)S + XS_x & XS_\kappa \\ \omega h & -\omega \end{pmatrix}. \tag{S6.3}$$

At an interior equilibrium, $S = 0$, so $J_{11} = XS_x$. Local asymptotic stability requires $\operatorname{tr} J = XS_x - \omega < 0$ and $\det J = -\omega X(S_x + hS_\kappa) > 0$. Since $\mathcal{F}'(x) = S_x + hS_\kappa$ after substituting

$\kappa = \kappa_{\mathrm{D}} + hx$, the determinant has the compact form

$$\det J = -\omega X \mathcal{F}'(x). \tag{S6.4}$$

With the present definition of $\mathcal{F} = S(x, \Psi(x))$, a physical interior state is a saddle when $\mathcal{F}'(x) > 0$ and can be stable or unstable when $\mathcal{F}'(x) < 0$. This identity was also used to cross-check numerical root classification.

For the proportional induced branch, it is sometimes convenient to use H in Eq. (S5.2). Because $S = D(1-\kappa(x-1/2)D)$, the determinant can equivalently be expressed in terms of DH'. Both implementations return the same classification away from degeneracies.

7 Saddle-node and Hopf bifurcations

7.1 Fold condition

A non-degenerate interior saddle-node of the general model satisfies $\mathcal{F}(x) = \mathcal{F}'(x) = 0$, with $\mathcal{F}''(x) \neq 0$ and a non-zero derivative with respect to the unfolding parameter. In the proportional induced branch this becomes $H = H' = 0$. Boundary collisions occur when an interior root reaches $x = 0$ or $x = 1$ and are governed by the corresponding invasion eigenvalue.

7.2 Hopf condition

At a fixed interior root, varying ω leaves (x_e, κ_e) unchanged. Let $A_e = XS_x$ and $B_e = XS_\kappa$ evaluated at that root. The trace and determinant are $A_e - \omega$ and $-\omega(A_e + hB_e)$. A Hopf candidate therefore requires

$$\omega_{\mathrm{H}} = A_e > 0, \qquad A_e + hB_e < 0. \tag{S7.1}$$

The trace crossing is transversal because $\partial_\omega \operatorname{tr} J = -1$. If $h = 0$, the determinant at $\omega = A_e$ is $-A_e^2 < 0$; strategy-dependent volatility is consequently necessary for this response-rate Hopf mechanism.

7.3 First Lyapunov coefficient

Translate the Hopf equilibrium to the origin and write the vector field as $\dot{z} = Az + B(z,z)/2 + C(z,z,z)/6 + \cdots$. Let $Aq = \mathrm{i}\Omega q$, $A^{\mathsf{T}} p = -\mathrm{i}\Omega p$, and normalize the complex inner product so that $\langle p, q\rangle = 1$. We use

$$\begin{aligned} l_1 = \frac{1}{2\Omega} \operatorname{Re} \big\langle p, C(q,q,\bar{q}) - 2B\left(q, A^{-1}B(q,\bar{q})\right) \\ + B\left(\bar{q}, (2\mathrm{i}\Omega I - A)^{-1} B(q,q)\right)\big\rangle . \end{aligned} \tag{S7.2}$$

Under this convention, $l_1 < 0$ and a trace that decreases through zero as ω increases correspond to a supercritical stable cycle on the $\omega < \omega_{\mathrm{H}}$ side. The code constructs the derivative tensors analytically from the polynomial vector field and checks the result by direct integration.

8 Exact proportional Hopf example

The parameter set

$$F = -\frac{530}{63}, \quad G = -\frac{2480}{63}, \quad \kappa_{\mathrm{D}} = \frac{91}{400}, \quad \kappa_{\mathrm{C}} = \frac{3}{400} \tag{S8.1}$$

has an induced equilibrium at $(x_{\mathrm{H}}, \kappa_{\mathrm{H}}) = (1/8, 1/5)$. Analytic substitution gives $\omega_{\mathrm{H}} = 5/12$ and Hopf frequency $\Omega = 0.7034142923$. Equation (S7.2) gives $l_1 = -18.50849634$. Direct cycles at $\omega/\omega_{\mathrm{H}} = 0.995, 0.99, 0.98$ and 0.97 have strategy half-amplitudes $0.01820, 0.02643, 0.04007$ and 0.05584, respectively. A fit of amplitude squared against $\omega_{\mathrm{H}} - \omega$ gives slope 0.26562 and $R^2 = 0.97666$, consistent with local normal-form scaling over this resolved interval.

At $\omega/\omega_{\mathrm{H}} = 0.95$, the chosen initial condition is instead captured by the defection boundary. This does not contradict the local supercritical result: the small stable cycle exists near onset, whereas global basin geometry changes farther away. The phase map in the main text therefore uses direct long-time classification in addition to the analytic Hopf curve.

9 Non-proportional sensitivity

The general model was tested in two ways. First, around the proportional multistable parameter set $F = -7.6446543172$, $G = 14.6579883311$, $\kappa_{\mathrm{D}} = 3.9727962202$, $\kappa_{\mathrm{C}} = 0.1098256080$ and $\omega = 0.2995504678$, we varied $P = pF$ and $Q = qG$ over $p, q \in [0.80, 1.25]$. Among 10,201 grid points, 4,571 retained four physical interior roots and at least two stable interiors.

Second, a qualitatively non-proportional Hopf example used $F = 12.73$, $G = 7.91$, $P = -7.98$, $Q = 5.11$, $\kappa_{\mathrm{D}} = 0.068$ and $\kappa_{\mathrm{C}} = 4.97$. The mean payoff and sensitivity differences have different signs and are not scalar multiples. The Hopf equilibrium is at $x = 0.8412351$, $\kappa = 4.1917345$ and $\omega_{\mathrm{H}} = 0.6569025$. The first Lyapunov coefficient is -0.8725391, and integration at $0.97\omega_{\mathrm{H}}$ gives a stable cycle with strategy amplitude 0.0865056.

10 Fast and slow environmental limits

For $\omega \gg 1$, Tikhonov reduction gives $\kappa = \Psi(x) + \mathcal{O}(\omega^{-1})$. The leading strategy equation is

$$x' = x(1-x)\left[F + Gx + \left(\tfrac{1}{2} - x\right)(\kappa_{\mathrm{D}} + hx)(P + Qx)^2\right], \tag{S10.1}$$

so its interior roots are precisely those of $\mathcal{F}$. Because the leading reduction is one-dimensional, it cannot contain a regular limit cycle. Oscillations in the full system require a finite response time.

For $\omega \ll 1$, introduce slow time $T = \omega\theta$. The fast layer holds κ fixed while x approaches stable branches of $S(x, \kappa) = 0$ or an invariant boundary. Volatility then drifts according to $\mathrm{d}\kappa/\mathrm{d}T = \Psi(x) - \kappa$. Folds of the critical manifold can generate rapid strategy jumps, while slow motion along distinct stable branches produces long transients and pronounced history dependence. These limits explain why the response ratio changes transient morphology even when equilibrium positions are unchanged.

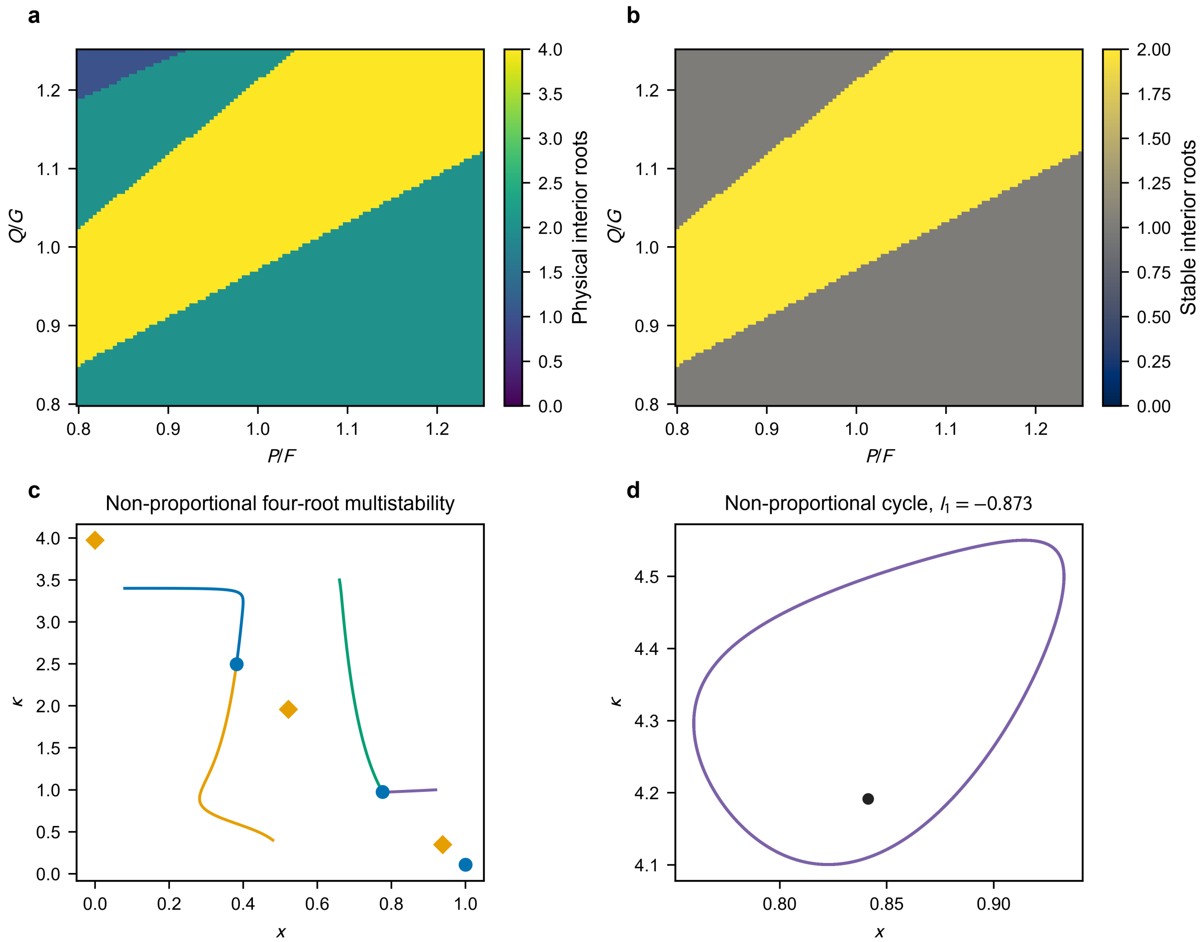

Supplementary Figure S1: **Robustness to non-proportional payoff sensitivity. a,b**, Number of physical and stable interior equilibria as the sensitivity intercept and slope are varied independently around the proportional multistable example. **c**, Four interior equilibria for a representative $B \neq A$ parameter set. **d**, Stable cycle in the strongly non-proportional Hopf example.

11 Finite-population absorption and effective size

For the diffusion in Eq. (S3.6), $x = 0$ and $x = 1$ are absorbing. Let $u(x, \kappa)$ be the probability of eventual absorption at all cooperation. Its backward equation is

$$b_x\, u_x + b_\kappa\, u_\kappa + \frac{x(1-x)}{s(N-1)} u_{xx} = 0, \qquad u(0,\kappa) = 0, \quad u(1,\kappa) = 1, \tag{S11.1}$$

where b_x and b_κ are the deterministic components of Eq. (S3.6). The corresponding mean absorption time solves the same operator equation with right-hand side -1 and zero boundary values. These two-dimensional boundary-value problems are not needed for the reported survival estimates, which were obtained directly from ensembles, but they define the exact diffusion observables.

In selection time, the leading demographic intensity depends on Ns. Accordingly, diffusion trajectories at fixed Ns collapse exactly within the leading approximation. The microscopic process has additional s- and N-dependent corrections. For $Ns = 10$, the survival RMSE between microscopic and diffusion ensembles decreased from 0.09518 at $(N, s) = (100, 0.1)$ to 0.08120 at $(200, 0.05)$ and 0.04713 at $(500, 0.02)$. This is the expected joint large-population, weak-selection convergence.

12 Shock-distribution robustness

Gaussian, Rademacher, uniform and Laplace variables were standardized to zero mean and unit variance. Exact transition expectations were computed over 51 composition–volatility combinations at four selection strengths, producing 204 distribution-level records. At $s = 0.02$, normalized drift RMSE ranged from approximately 0.00246 to 0.00251, and the maximum shift of the inferred equilibrium across distributions was 9.5003×10^{-5}. Supplementary Fig. S2d subtracts the Gaussian drift to expose the higher-order differences that are hidden when the curves overlap.

13 Numerical convergence

The finite-N diffusion coefficient was tested for N from 20 to 3,000. The measured quantity $N^2\,\mathrm{Var}(\Delta x)$ followed the exact no-self-interaction result and approached $2x(1-x)$ with relative correction $1/(N-1)$. Deterministic cycle calculations were repeated with $(\mathrm{rtol}, \mathrm{atol}, \mathrm{max\ step})$ equal to $(10^{-8}, 10^{-10}, 0.20)$, $(2 \times 10^{-10}, 10^{-12}, 0.12)$ and $(10^{-11}, 10^{-13}, 0.06)$. Relative to the strictest setting, the amplitude deviations are of order 10^{-9}; the detected periods are identical at the recorded precision.

14 Parameter sets used in the figures

The payoff-plane figure uses $F, E \in [-10, 10]$ and $G = E - F$ at fixed environmental parameters from the multistable set. The sensitivity-robustness map uses $P/F, Q/G \in [0.80, 1.25]$. The Hopf phase map uses the exact proportional mean-payoff parameters while varying h and ω as recorded in the exported CSV file. All plotted coordinates and class labels can be regenerated

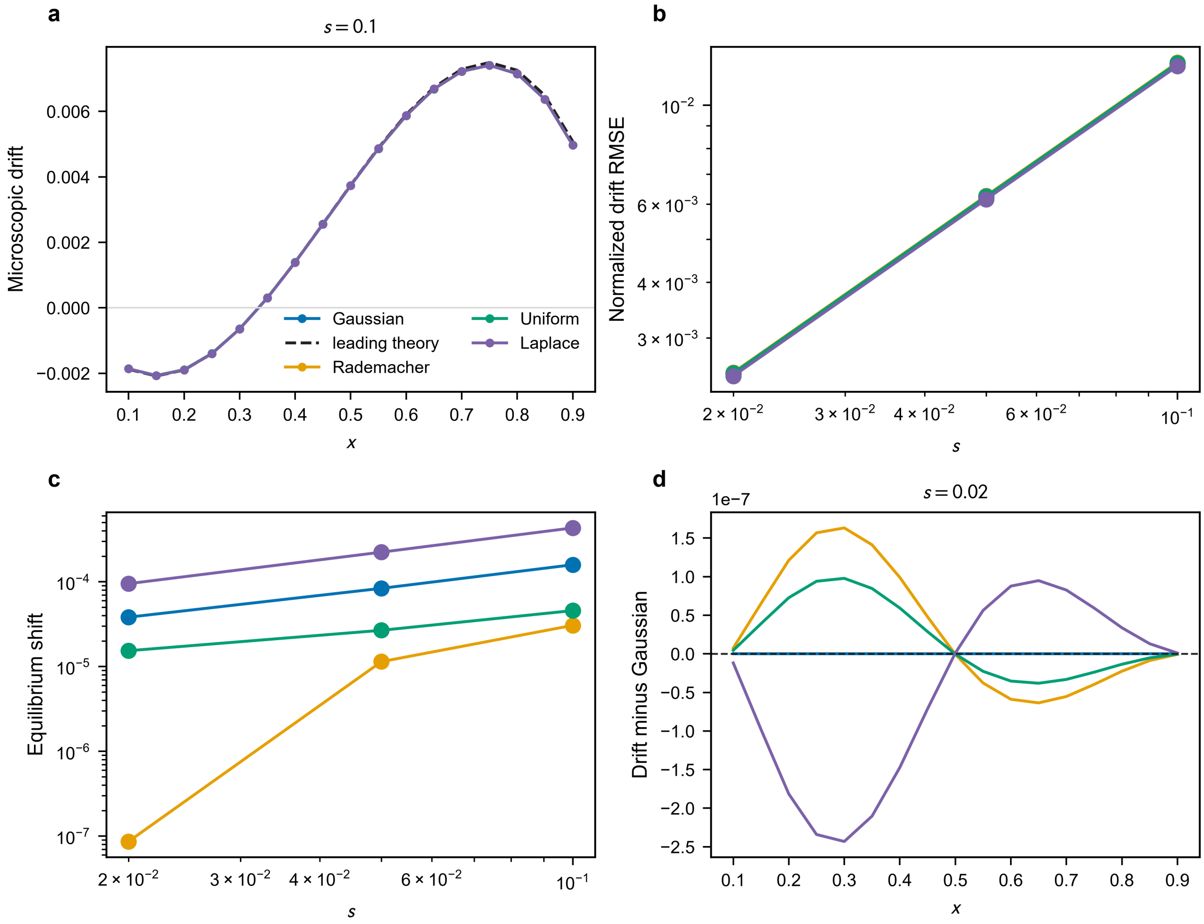

Supplementary Figure S2: **Robustness to the distribution of fast payoff shocks.** **a**, Exact microscopic drift for four centered, unit-variance distributions at $s = 0.1$, with the common leading theory. **b**, Weak-selection convergence of normalized drift error. **c**, Absolute equilibrium displacement from the leading prediction. **d**, Distribution-specific drift minus the Gaussian result at $s = 0.02$, revealing only higher-order differences.

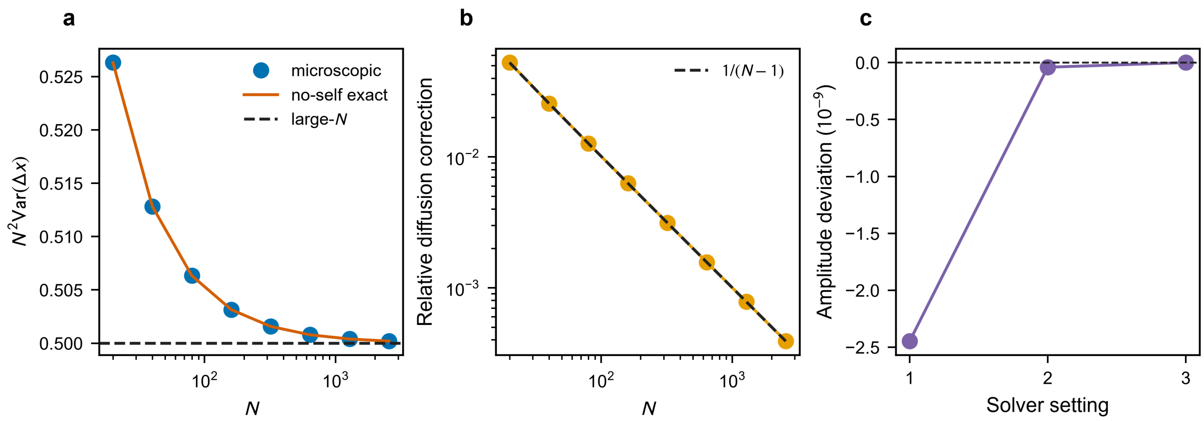

Supplementary Figure S3: **Finite-population and solver convergence.** **a**, Microscopic one-step variance and the exact no-self-interaction expression. **b**, Relative correction to the large-N diffusion coefficient, with the analytic $1/(N-1)$ guide. **c**, Cycle-amplitude deviation, in parts per billion, across three solver settings.

Supplementary Table S2: Deterministic parameter sets. Decimal values are recorded at the precision used by the code.

Use	F	G	P	Q	κ_D	κ_C	ω
Multistable proportional	-7.644654	14.657988	F	G	3.972796	0.109826	0.299550
Exact proportional Hopf	$-530/63$	$-2480/63$	F	G	91/400	3/400	5/12 at Hopf
Non-proportional Hopf	12.73	7.91	-7.98	5.11	0.068	4.97	0.656902 at Hopf

from those tables without digitizing the figures.

15 Random seeds and simulation counts

Supplementary Table S3: Stochastic provenance.

Calculation	Replicates	Seed rule or source
Main finite-population survival	900 per N	20260824+97i, where i indexes increasing population size
Conditional occupation density	900	same seed as the $N = 10^4$ survival ensemble
Fixed-Ns exact birth–death	120 per pair	fixed seeds recorded by `scripts/analyze_robustness.py`
Fixed-Ns diffusion reference	4,000	fixed seed recorded by `scripts/analyze_robustness.py`
Microscopic drift validation	independent draws plus quadrature	quadrature values are deterministic; Monte Carlo seed is fixed in the validation script
Search provenance	deterministic fixed-seed search	candidate tables are exported as CSV and rechecked analytically

16 Approximation scope and excluded claims

The drift reduction assumes $s \ll 1$, finite shock moments sufficient for the expansion, and independent shocks at the microscopic scale. The deterministic model additionally assumes demographic diffusion is negligible on the observation horizon. The finite-population diffusion assumes increments are small relative to the strategy interval and becomes inaccurate for strong selection or very small N. None of the analyses establishes universality for infinite-variance shocks, temporally persistent shocks, spatially correlated environments, nonlinear payoff-to-fitness maps outside the local expansion, or arbitrary update rules.

The parameter scans establish existence and robustness within explicitly reported windows; scan fractions are not probabilities over games. Basin percentages refer to uniform sampling of a displayed rectangle and are not empirical frequencies. The negative Lyapunov coefficient establishes the local Hopf criticality for the given convention, while direct integration verifies stable cycles over a finite parameter band. Finally, all points formerly described as an unresolved region in the proportional endpoint-payoff map lie on the non-hyperbolic axes $F = 0$ or $E = 0$; no finite-area oscillatory region is claimed from that scan.